Rare Met. (2021) 40(11):3269–3278
https://doi.org/10.1007/s12598-021-01763-8

RARE METALS

ORIGINAL ARTICLE

Synchrotron X-ray diffraction characterization of phase transformations during thermomechanical processing of a Ti38Nb alloy

Qing-Kun Meng, Huan Li, Chong-Hang Zhao, Wen Ma*, Fu-Xiang Wei, Yan-Wei Sui, Ji-Qiu Qi*

Received: 13 January 2021 / Revised: 28 February 2021 / Accepted: 3 March 2021 / Published online: 25 May 2021

Abstract The phase transformations during thermomechanical processing can be employed to optimize mechanical properties of β-type Ti alloys. However, such understandings are still lacking for the alloy consisting of dual β + α″ phases in solution-treated and quenched state. In this paper, the phase transformations in a Ti38Nb model alloy subjected to different thermomechanical processing were investigated by using synchrotron X-ray diffraction (SXRD) experiments, and their influence on the Young's modulus was discussed. The results indicated that high-density dislocations introduced by cold rolling still existed after annealing at temperatures lower than 573 K, which can decrease the martensitic transformation start temperature to below room temperature. With annealing temperatures increasing, the α″ → β, β → ω_{iso}, and β → α phase transformations occurred successively. At annealing temperature of 473 K, the specimen consisted of a trace of α″ and ω phases as well as dominant β phase which was kept to room temperature by the high density of dislocations, rather than by the chemical stabilization. As a result, an ultralow Young's modulus of 25.9 GPa was realized. Our investigation not only provides in-depth understandings of the phase transformations during thermomechanical processing of β-type Ti alloys, but also sheds light on designing biomedical Ti alloys with ultralow Young's modulus.

Keywords Ti alloys; Phase transformation; Thermomechanical processing; Synchrotron X-ray diffraction

1 Introduction

Titanium (Ti) and its alloys have become one of the most attractive classes of biomedical implant materials due to their low density, good mechanical properties, superior corrosion resistance, excellent biocompatibility, and low Young's modulus [1, 2]. Compared with other metallic biomaterials such as Co–Cr alloys and stainless steels with modulus higher than 200 GPa, the α-type Ti and (α + β)-type Ti–6Al–4V alloy have moduli of about 104 and 110 GPa, respectively [3]. The lower modulus is beneficial to reduce the stress shielding effect which is caused by the modulus mismatch between human bones and implants [4, 5]. However, the Young's modulus of pure Ti and Ti–6Al–4V alloy is still much higher than that of human bone (10–30 GPa), and the stress shielding effect would lead to bone resorption and premature failure of implants [6]. Besides, toxicity of Al and V in Ti–6Al–4V alloy is concerned [2]. These drawbacks have motivated the development of novel β-type Ti alloys with lower modulus and greater biocompatibility. As a result, various biomedical β-type Ti alloys have been fabricated by alloying Ti with nontoxic elements, e.g., binary TiNb [7], TiMo [8], TiTa [9], ternary TiNbSn [10, 11], TiNbZr [12, 13], quaternary TiNbTaZr [14, 15], TiNbZrSn [16, 17].

Q.-K. Meng, H. Li, F.-X. Wei, Y.-W. Sui, J.-Q. Qi*
School of Materials Science and Physics, China University of Mining and Technology, Xuzhou 221116, China
e-mail: qijiqiu@cumt.edu.cn

C.-H. Zhao
Department of Materials Science and Chemical Engineering, Stony Brook University, Stony Brook, NY 11794, USA

W. Ma*
Grinm Group Co., Ltd., Beijing 100088, China
e-mail: mawen@grinm.com

The metastable β-type Ti alloys have two stable phases, including the bcc β phase at high temperatures and the hcp α phase at lower temperatures [18]. In addition, metastable hcp α′ martensite or orthorhombic α″ martensite might form after quenching from above β-transus temperature, with lower and higher β stabilizer concentration corresponding to the formation of α′ and α″ phases, respectively [19]. The martensitic transformation start temperature (M_s) is affected by the content of β stabilizing elements, and M_s can be decreased to below room temperature above a critical β stabilizer concentration (denoted as β_c hereafter) [20, 21]. When quenching β-type Ti alloys with the composition around β_c, metastable athermal ω particles (ω_{ath}) usually formed by a diffusionless shuffle transformation [22]. It has been reported that the collapse of $(111)_\beta$ planes creating the ω phase may be only partial during quenching and the size of the ω_{ath} particles is quite small (typically several nanometers) [23]. Upon annealing, isothermal ω particles (ω_{iso}) further evolve by an irreversible diffusive transformation during which β stabilizers are rejected from ω_{iso} particles to the surrounding β-matrix and a complete collapse of $(111)_\beta$ planes takes place simultaneously [24].

Among the phases of β, α, α″ and ω, it is well accepted that the ω phase has the highest Young's modulus and the α phase has a higher modulus than the β phase [25]. Although few researches indicated that the α″ martensite had the lowest modulus among α′, α″, α and β phases in binary TiMo system [26], it was generally recognized that the β phase exhibited the lowest modulus among all the phases in Ti alloys [27, 28]. Furthermore, the Young's modulus is determined by the phase stability and decreases with the decrease in β phase stability [28]. The lowest modulus can be realized in a least stable β phase by adding β stabilizers as less as possible. Consequently, most of the low-modulus Ti alloys contain a β stabilizer concentration slightly higher than β_c to stabilize single β phase against α″ and ω phase transformations. Based on the above strategy, various β-type Ti alloys with Young's modulus have been developed through careful composition design [3].

In order to enhance the mechanical properties of low-modulus Ti alloys, various thermomechanical processing methods have been applied, e.g., cold rolling, warm rolling, hot forging, annealing and solution treatment [29–33]. However, most studies have been carried out for alloys with composition above β_c, the thermomechanical processing of β-type Ti alloys with β stabilizer concentration below β_c is seldom studied. Furthermore, the current researches focus on the influence of the ω and α precipitation on the mechanical properties [34, 35], while the α″ → β reverse martensitic transformation and its influence on the mechanical properties during thermomechanical treatments remain ambiguous.

It is well known that the conventional X-ray diffraction (XRD) identifies the phase constituent within 20–30 μm near the surface of samples. However, the surface effect of phase transformation might exist during quenching of β-type Ti alloys, which makes it difficult to obtain the accurate phase constituent of the entire sample by conventional XRD [36]. For example, it has been reported that abundant α″ martensite phase formed in the surficial region, while dominant β phase together with a few ω phase existed in the interior after quenching of a β-type TiNbZr alloys [37]. Furthermore, it is difficult to identify small amount of α, α″ and ω phases from conventional XRD patterns due to the overlapping of diffraction peaks. In order to avoid these limitations, synchrotron X-ray diffraction (SXRD) can be used to trace the phase transformation in a small extent due to the high resolution [38–40]. Besides, the high penetration and low absorption of the synchrotron X-rays make it possible to identify the phase constitution of the entire sample by using a transmission diffraction geometry [41].

In this paper, a binary Ti38Nb (wt%) alloy was employed as a model system with β stabilizer concentration below β_c to study the phase transformations during thermomechanical processing. The one-dimensional (1D) and the corresponding two-dimensional (2D) SXRD spectrums were obtained to characterize the phase constituents of the entire samples. Special attention was focused on the α″ → β reverse martensitic transformation during low-temperature annealing and its influence on the Young's modulus of the alloy. Our results indicated that ultralow modulus equivalent to that of human bones could be realized by optimizing the phase constituent of the Ti38Nb alloy through appropriate thermomechanical processing.

2 Experimental

An ingot with a nominal composition of Ti38Nb (wt%) was fabricated by arc melting in an argon atmosphere using high purity Ti (99.99%) and Nb (99.95%). In order to obtain a homogeneous composition, the ingot was flipped and melts again, and the process was repeated four times. The ingot was forged at high temperature, and a billet with a cross section of 9 mm × 60 mm was finally fabricated. The billet was homogenized at 1223 K for 5 h in a vacuum quartz tube. After homogenization treatment, the billet was quenched into water by breaking the quartz tube. The billet was subjected to cold rolling (CR), and a plate with a thickness of 1 mm was finally obtained. The cold rolling reduction ratio is 89%. Specimens were cut from the CR plate using an electro-discharge machine. Part of CR specimens were solution treated at 1073 K for 1 h in an evacuated quartz tube and quenched into water by breaking

quartz tubes (denoted as ST hereafter). On the other hand, part of CR specimens were annealed at different temperatures from 373 to 673 K for 30 min and finally quenched into water (denoted as CRA hereafter). Uniaxial tensile test was conducted on an Instron 8801 machine at room temperature with a strain rate of 1×10^{-4} s^{-1}. Tensile specimens have a gauge length of 30 mm and a rectangular cross section of 1.00 mm × 1.46 mm, with the rolling direction parallel to the loading axis. The stress–strain curves were measured through a strain extensometer. Conventional XRD measurements were performed using a Rigaku D/max2550 diffractometer with Cu Kα radiation at an accelerating voltage of 40 kV and a current of 250 mA. Transmission electron microscopy (TEM) characterizations were performed using a JEOL 2100 microscope operating at 200 kV. Thin foils for TEM observations were prepared by a twin-jet electro-polishing technique in a solution of 4% perchloric acid in methanol at about 250 K.

SXRD experiments were conducted at the X-ray powder diffraction beamline (XPD, 28-ID-2) at National Synchrotron Light Source II (NSLS-II), Brookhaven National Laboratory. High-energy X-rays (energy of 64.17 keV, wavelength of 0.01932 nm, beam size of 0.5 mm × 0.5 mm) were used with the beamline perpendicular to the roll plane of the samples. A large-area amorphous-silicon digital X-ray detector of 2048 × 2048 pixels with a spatial resolution of 200 μm (pixel size) was placed behind the sample to collect the 2D diffraction images. The exposure time of each scan was 10 s per 2D image. A Ni standard was first used for calibration and the sample-to-detector distance was determined to be 1492.29 mm. The 1D SXRD patterns were obtained by azimuthally integrating over the entire diffraction rings using Dioptas software [42].

3 Results and discussion

3.1 XRD and tensile results of solution-treated and cold-rolled specimens

Figure 1a shows conventional XRD patterns of the solution-treated (ST) and cold-rolled (CR) specimens. Dual β + α″ phases can be clearly identified in the ST specimen, suggesting that the α″ martensitic transformation occurred during quenching the Ti38Nb alloy from the single β phase field. This indicates that the Nb concentration is below β_c and thus the martensitic transformation start temperature (M_s) is above room temperature in ST state. Upon cold rolling at a reduction ratio of 89%, the alloy still consists of dual β + α″ phases. As is well known, stress-induced martensitic transformation (SIMT) would take place during cold deformation of β-type Ti alloys with low phase stability [43, 44]. It is believed that the volume fraction of α″ martensite increased after cold rolling, although it is difficult to determine the accurate volume fractions before and after cold rolling from the current XRD patterns. Interestingly, the relative intensity of $(200)_{\alpha''}$ diffraction peak increases significantly after cold rolling, indicating the formation of α″ texture component with the (200) crystal plane parallel to the rolling plane.

Figure 1b shows the tensile stress–strain curves of the ST and CR specimens. The ST alloy exhibits a typical double yielding phenomenon, with the first yielding corresponding to SIMT and/or the reorientation of the martensite variants, and the second yielding to the initiation of dislocation slip. Apparently, the β-type Ti alloys with β stabilizer concentration below β_c are not suitable for biomedical applications in ST state because of the quite low yielding plateau stress. The double yielding phenomenon disappears after cold rolling, suggesting that the SIMT and/or the reorientation of the martensite variants were suppressed or even did not occur. Large amounts of defects including dislocations and grain boundaries can be introduced during severe deformation [45, 46]. This can hinder the α″ martensitic transformation upon loading and lead to the disappearance of double yielding phenomenon. If the SIMT was completely suppressed for the CR specimen, the deformation mode is dislocation slip. However, recent researches indicated that SIMT in small extent still existed in some metastable β-type Ti alloys during loading even though these alloys did not exhibit double yielding phenomenon [47]. Therefore, the SIMT in small extent and/or dislocation slip is the deformation modes of the CR specimen. As a result, the yielding strength of the Ti38Nb alloy was significantly improved by high-density defects introduced during cold rolling.

Interestingly, the CR specimen exhibits a lower Young's modulus of 45 GPa in comparison with 59.5 GPa for the ST specimen. The Young's modulus is determined by the phase constitution and the modulus of each individual phase. It is worth noting that both β phase and α″ martensite in Ti alloys show Young's modulus anisotropy in different crystal directions. Therefore, the texture evolution during cold rolling might also play an important role in the Young's modulus. It was reported that $(200)_{\beta}$ $<110>_{\beta}$ and $(200)_{\alpha''}[010]_{\alpha''}$ texture usually formed during severe cold deformation of metastable β-type Ti alloys [48]. Furthermore, both the $<110>_{\beta}$ and $[010]_{\alpha''}$ crystal directions have relatively lower Young's modulus [48, 49]. It will be demonstrated that the β phase of the present alloy has lower modulus in the following context. Therefore, the increase in the volume fraction of the α″ martensite after cold rolling will lead to the increase in Young's modulus. However, this was compensated by the decrease in Young's modulus caused by the formation of

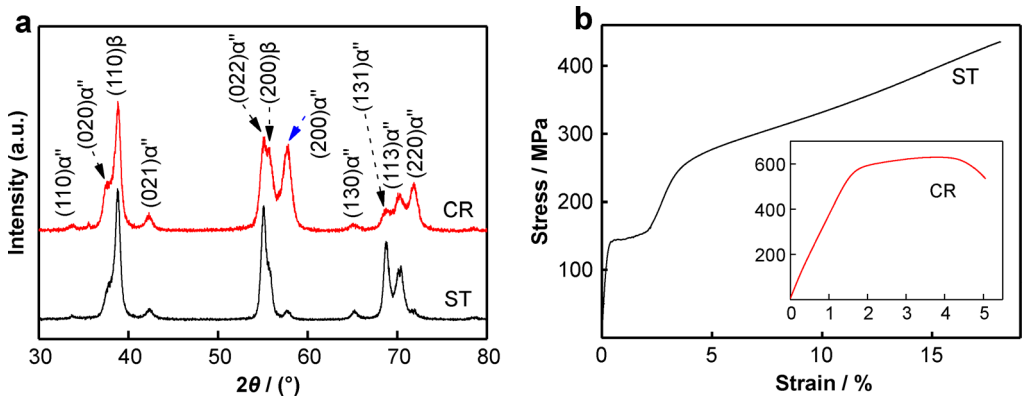

Fig. 1 **a** Conventional XRD patterns and **b** tensile stress–strain curves of solution treated (ST) and cold rolled (CR) specimens

texture and the elastic modulus anisotropy. As a result, the Young's modulus decreased after cold rolling.

3.2 SXRD and TEM characterization of cold-rolled plus annealed specimens

To study the phase transformations during the thermomechanical processing of the Ti38Nb alloy, the CR specimens were annealed at different temperatures from 373 to 673 K for 30 min, followed by quenching into water (CRA). Figure 2 shows 1D SXRD patterns of the CRA-treated specimens and corresponding 2D SXRD images of four typical samples are present in Fig. 3. It can be seen from Figs. 2, 3a that CR specimen consists of dual $\beta + \alpha''$ phases, consistent with the conventional XRD results. After annealing at 373 K, the SXRD pattern remains almost the same to that of CR specimen, suggesting that no obvious phase transformation occurred at this temperature. It was reported that the reverse martensitic start temperature (A_s) and the reverse martensitic finish temperature (A_f) were about 358 and 428 K for a ST Ti38Nb alloys, respectively [50]. Apparently, the reverse martensitic transformation of the present alloy was retarded by cold rolling. The martensitic transformation from the β phase to orthorhombic α″ includes three individual processes [18]. Firstly, the cubic lattice transforms to the orthorhombic lattice through Bain distortion. Secondly, the invariant plane is realized by the lattice invariant shear. Finally, the atoms are brought to their positions in the orthorhombic lattice through a shuffle on every alternate (110) plane in a $[1\bar{1}0]$ direction. The martensitic transformation process including the Bain distortion, shear and shuffle can be hindered by the crystal defects in different size scales [51]. These defects involve interstitial atoms, substitutional atoms, dislocations, phase interfaces, grain boundaries, secondary precipitates, etc. The severe cold deformation resulted in the grain refinement of both β phase and α″ martensite in addition to the increase in dislocation density [52]. The large amount of dislocations, grain boundaries and phase interfaces can hinder significantly the martensitic and reverse martensitic transformation [25, 48]. Therefore, the higher A_s of the present CR Ti38Nb alloy might be attributed to the large amount of defects introduced by cold rolling.

After annealing at 423 K, the alloy still exhibits dual $\beta + \alpha''$ phases, while the relative intensities of β and α″ diffraction peaks change slightly, suggesting that slight $\alpha'' \rightarrow \beta$ reverse martensitic transformation occurred during annealing treatment and the A_s of the present alloy was supposed to be in the range of 373–423 K. The α″ diffraction peak intensities decrease drastically after annealing at 473 K, and the alloy consists of dominated β phase together with a trace of α″ martensite, as shown in Figs. 2c, 3b. By carefully analyzing the 2D SXRD image in Fig. 3b, a diffuse zone marked by a red rectangle can be identified between $(220)_\beta$ and $(132)_{\alpha''}$ diffraction rings, which results in the formation of a rather broad peak alongside the $(132)_{\alpha''}$ diffraction peak in the 1D SXRD pattern (Fig. 2e). Furthermore, there also exists a diffuse zone in the 2D SXRD image of the CR specimen (Fig. 3a) which is located just inside the $(220)_\beta$ diffraction rings. Such diffuse zone does not appear at an annealing temperature of higher than 473 K. It is assumed that the diffuse zone is ascribed to the ω_{ath} phase with a small size and low volume fraction. Athermal ω phase could be formed during quenching of the metastable β-type Ti alloy [53]. On the other hand, the ω_{iso} precipitation requires sufficient thermal activation, i.e., exposure to high enough temperatures [54]. Therefore, the $\beta \rightarrow \omega_{iso}$ phase transformation might not occur or just take place to a small extent for specimens annealed at 473 K or lower.

By further increasing the annealing temperature to 523 K, diffraction peaks ascribed to α″ martensite vanish, suggesting the completion of the $\alpha'' \rightarrow \beta$ reverse martensitic. Meanwhile, clear $(112)_\omega$ diffraction peak can be identified from the enlarged view of the 1D SXRD pattern

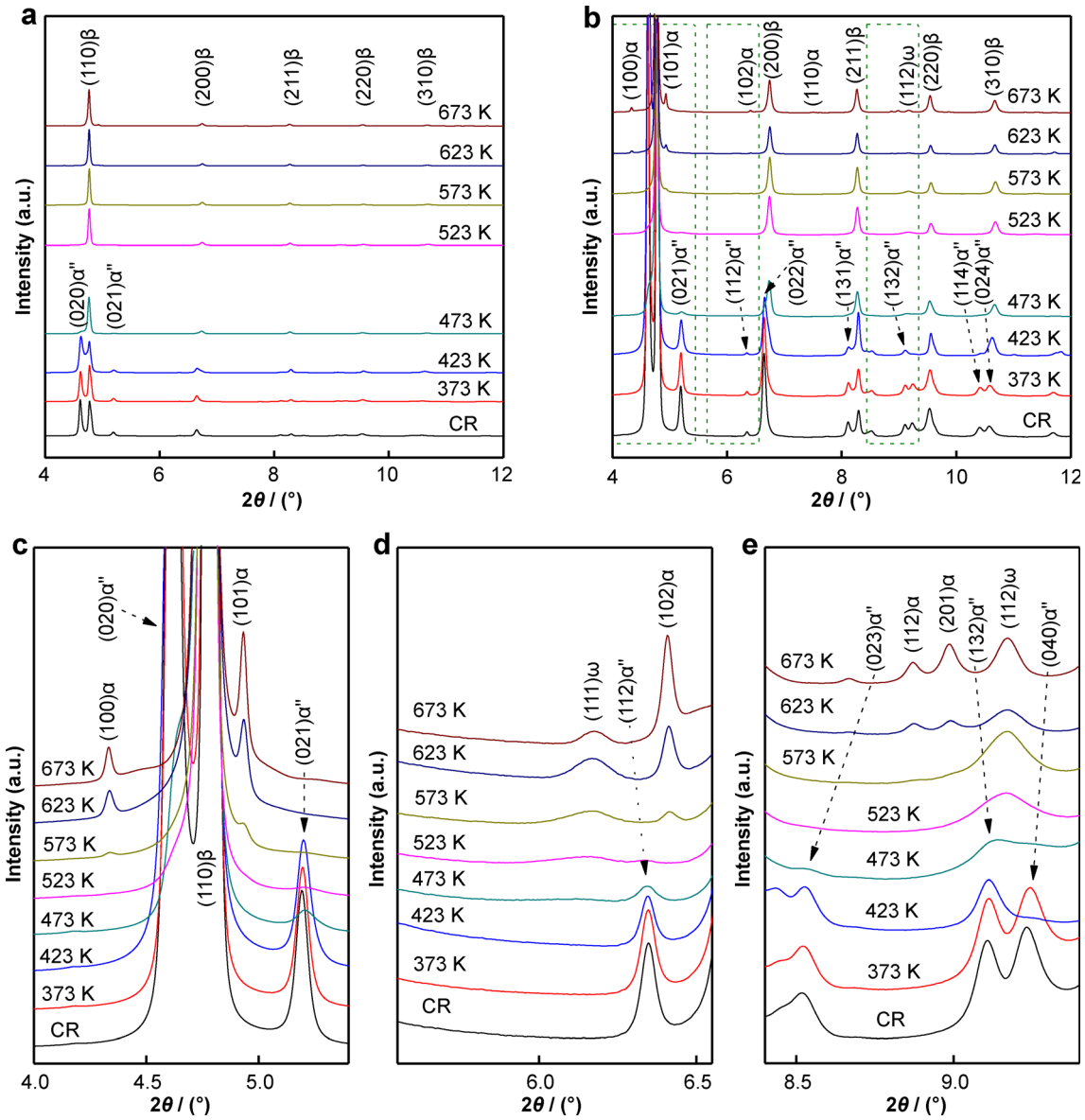

Fig. 2 **a**, **b** 1D SXRD patterns of specimens subjected to different thermomechanical processing; **c–e** enlarged views of boxed areas in **b**

(Fig. 2e), implying that the precipitation of ω_{iso} occurred at 523 K. After annealing at 573 K, weak peaks ascribed to (100) and (101) crystal planes of the α phase appeared and the alloy was composed of β, α and ω phases (Fig. 2c–e). Furthermore, the diffraction peak intensities of $(111)_{\omega}$ and $(112)_{\omega}$ peaks increased in comparison with those after 523-K annealing. Figure 3c shows that clear $(112)_{\omega}$ diffraction ring formed rather than a diffuse zone, indicating the increasing volume fraction and size of the ω_{iso} phase. Different from the ω_{ath} phase with a diameter of several nanometers, the ω_{iso} can grow in size by a factor of 10 or more [55]. With the annealing temperature further increasing to 623 and 673 K, the relative diffraction intensities of the α phase increased clearly, indicating the increasing volume fraction of the α precipitates (Fig. 2c). However, the diffraction peak intensities of the ω phase did not show a clearly increase with the increase in the annealing temperature to 623 and 673 K (Fig. 2d,e). Previous investigations indicated the ω_{iso} phase can precipitate at a lower temperature, while α phase precipitation will become dominant and the ω_{iso} will be either dissolved into β phase or transformed into α phase at a higher temperature or a longer time [56]. For the present CR Ti38Nb alloy, the above results indicated that β → ω_{iso} phase transition was the dominant diffusive transformation at annealing temperatures of 523–573 K, whereas the precipitation of α phase was more significant than that of the ω_{iso} phase at higher temperatures of 623 and 673 K.

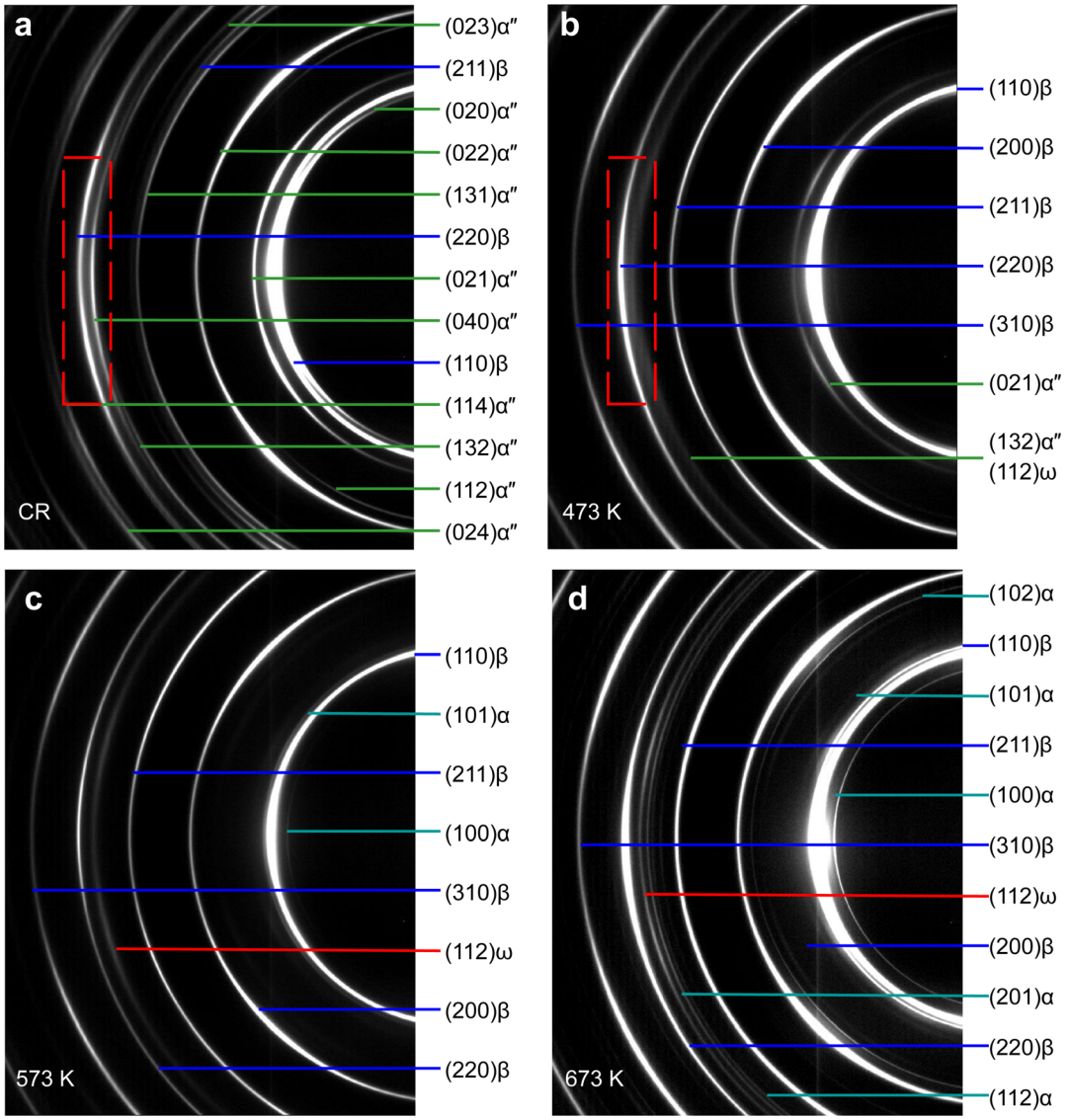

Fig. 3 2D SXRD patterns of **a** CR specimen and specimens annealed at **b** 473 K, **c** 573 K and **d** 673 K for 30 min

TEM characterizations of the ST specimen have been performed in our previous study [57]. In brief, the lath-shaped α″ martensite as well as the nanosized athermal ω precipitates was homogeneously distributed within the β parent phase of the ST Ti38Nb alloy. Furthermore, our results indicated that cold rolling would lead to significant grain refinement and introduce large amount of dislocations for β-type Ti alloys with β stabilizer concentration below β_c, which should also occur during cold rolling of the present Ti38Nb alloy [12, 58, 59]. In order to further study the microstructural evolution during thermomechanical processing, Fig. 4 shows TEM images of the CR specimens annealed at 473 and 573 K. The low-magnification bright-field image of the 473 K annealed specimen (Fig. 4a) shows apparent contrast presumably caused by dislocation tangles, suggesting that fully recrystallization did not occur after annealing. These dislocation tangles were supposed to be introduced by the severe cold rolling prior to annealing, which can suppress the α″ martensitic transformation during quenching [60]. It is assumed that the M_s of the present 473 K annealed specimen is below room temperature. While extensive α″ → β reverse martensitic transformation occurred during annealing, β → α″ martensitic transformation did not occur during subsequent quenching, leading to a phase constituent of dominate β phase and a trace of α″ martensite (Fig. 2). By sharp contrast, annealing above A_s and quenching a dual (β + α″) Ti alloy in ST state would reproduce the initial martensitic state [61]. Apparently, α″ → β reverse martensitic transformation took place during annealing above the A_s and β → α″ martensitic transformation occurred during quenching, if the martensitic

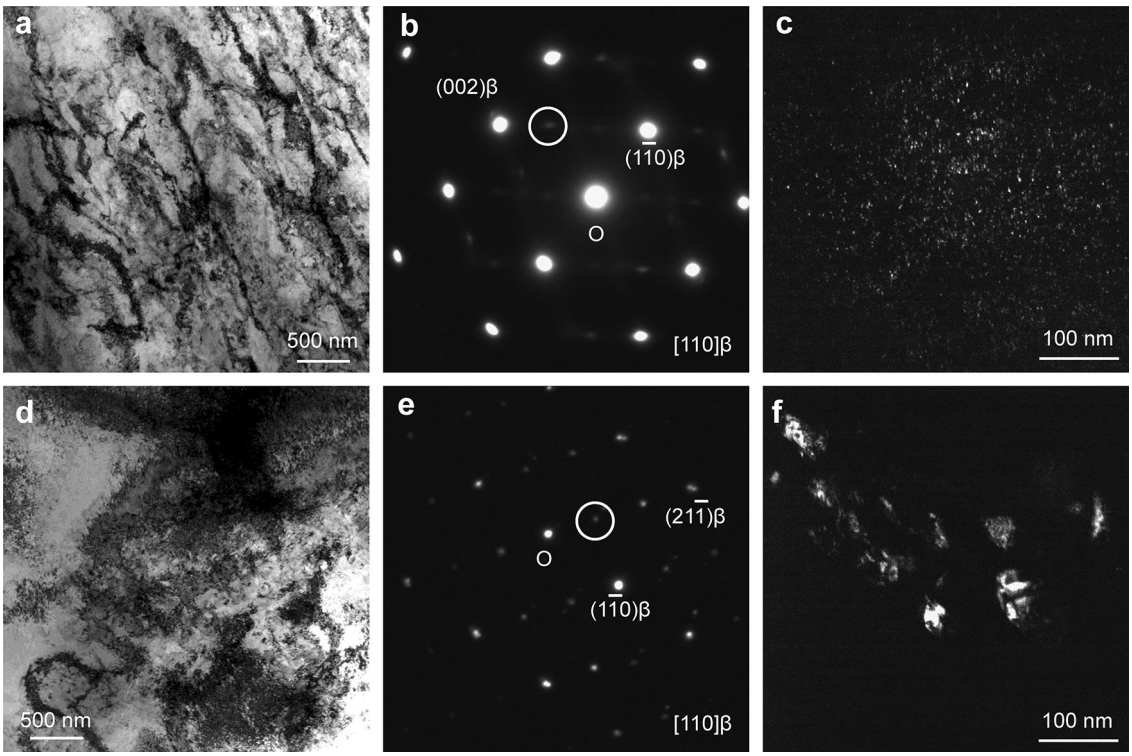

Fig. 4 **a** Low-magnification bright-field TEM image, **b** SAD pattern and **c** corresponding dark–field TEM image of specimen annealed at 473 K for 30 min; **d** low-magnification bright-field TEM image, **e** SAD pattern and **f** corresponding dark–field TEM image of specimen annealed at 573 K for 30 min

transformation was not suppressed by the microstructure changes or chemical stabilization of the β phase.

Figure 4b shows selected area diffraction (SAD) pattern recorded along the <110> zone axis of the β phase. Weak reflections at the 1/3 and 2/3 $\{112\}_\beta$ positions can be identified, suggesting the existence of the ω phase. Figure 4c shows a dark-field TEM image by using one of the ω reflections marked by the white circle in Fig. 4b. It can be seen that the ω particles in sub-10 nm scale are uniformly distributed throughout the β matrix. Owing to the small size and uniform distribution, these ω particles can be ascribed to the athermal ω phase or the early stages of the isothermal ω phase whose composition is far from equilibrium [23].

Figure 4d shows low-magnification bright-field image of the 573-K-annealed specimen. Apparent contrast caused by dislocation tangles still exists, indicating the incompletion of recrystallization after annealing. The $<110>_\beta$ zone axis SAD pattern clearly exhibits distinct ω reflections at the 1/3 and 2/3 $\{112\}_\beta$ positions (Fig. 4e). Dark-field TEM image using one of the ω reflections marked by the white circle in Fig. 4e is shown in Fig. 4f. Well-developed and comparatively coarse ω particles with a diameter of ~ 50 nm are visible in the dark-field image, revealing that the growth of ω_{iso} particles is significant after annealing at 573 K. Different from the ω_{ath}, the formation of ω_{iso} can expel the β stabilizers into the surrounding β-matrix, resulting in the chemical stabilization of the residual β phase [24]. Furthermore, the ω_{iso} phase has higher volume fractions than the ω_{ath} phase, as shown in the SXRD patterns of specimens annealed at 473 and 573 K (Fig. 2d, e). Therefore, the precipitation of ω_{iso} is detrimental to achieve low Young's modulus due to above two aspects. As for the 573-K-annealed sample, the α phase was not observed from the TEM images. In fact, the precipitation of the α phase cannot be verified by the conventional XRD results. Thanks to the high flux of the synchrotron X-rays, weak diffraction peaks of the α phase can be identified from SXRD results (Fig. 2c). This implies that the volume fraction of the α precipitates is very low and the size is very small. Besides, the synchrotron X-rays have a beam size of 0.5 mm × 0.5 mm, while the thin foil that can be characterized by TEM is in the scale of micrometer size. Therefore, it is deduced that the small size of the α phase and/or the limited area for TEM observations led to the absence of α phase in the TEM images.

3.3 Evolution of mechanical properties during thermomechanical processing

In order to investigate the influence of phase transformations on the Young's modulus, uniaxial tensile tests were

carried out for specimens subjected to different thermomechanical processing. Figure 5 shows the tensile stress–strain curves and the corresponding Young's modulus determined from the initial linear region of the stress–strain curves. As described above, the Young's modulus decreased after cold rolling due to the formation the $(200)_{\alpha''}[010]_{\alpha''}$ texture and the $[010]_{\alpha''}$ crystal orientation with a lower modulus [48]. After annealing at 373 and 423 K, the Young's modulus remained similar to that of CR specimen, which agrees well with the SXRD results that the phase constituent remained almost unchanged. Interestingly, the Young's modulus of 473-K-annealed specimen decreased to an impressive low value of 25.9 GPa (equivalent to that of human bones). As the amount of the α'' phase decreased drastically after annealing at 473 K (Fig. 2), it can be demonstrated that the β phase has a lower modulus than the α'' martensite and the sharp decrease in the Young's modulus originated from the $\alpha'' \rightarrow \beta$ reverse martensitic transformation. The β phase of the present Ti38Nb alloy is expected to have an intrinsically low Young's modulus, since its β stabilizer concentration is below β_c. TEM iamge (Fig. 4c) indicates that the ω_{ath} phase or the early stages of the ω_{iso} phase formed after annealing at 473 K, and SXRD patterns (Fig. 2) demonstrated that the volume fraction of the ω phase was very low. Therefore, the formation of the ω phase was supposed to have subtle influence on the chemical stabilization of the β phase. In other words, the β phase can remain a similar composition after thermomechanical processing to that in ST state. Consequently, ultralow Young's modulus can be obtained by stabilizing the low modulus β phase to room temperature and controlling the amount of high modulus α'' martensite and ω phase.

Although the α'' martensite disappeared after annealing at 523 K, the Young's modulus increased to 36.9 GPa due to the precipitation of the ω_{iso} phase. The Young's modulus of the 573-K-annealed specimen is even higher (54.5 GPa), which is apparently caused by the increasing volume fractions of the ω_{iso} phase and the precipitation of the α phase. However, the Young's modulus remained similar with the annealing temperature further increasing to 623 and 673 K, although the volume fractions of the α phase increased clearly (Fig. 4c, e). At higher temperatures, the α phase preferred to precipitate at the expense of the ω phase [56]. Therefore, it is possible that the increase in the modulus caused by the α phase precipitation is compensated by the dissolution of the ω phase, resulting in the similar Young's modulus of specimens annealed at 573–673 K.

Based on the above results, a new strategy of designing β-type Ti alloys with ultralow Young's modulus is proposed. Firstly, an alloy with β stabilizer concentration below β_c is chosen so that the β phase can have intrinsically low modulus. Secondly, severe plastic deformation is applied to introduce high-density defects that can suppress the martensitic transformation. Finally, an annealing treatment is performed, during which the α'' martensitic formed during ST treatment and plastic deformation can transform back to the β phase and the precipitation of the ω and α phases is under control so that the β phase can remain the original composition. As a result, the ultralow Young's modulus might be realized in an alloy consisting of dominant β phase with composition below β_c. It should be recognized that the present CR plus annealed (573 K for 30 min) Ti38Nb alloy with ultralow Young's modulus is not suitable for practical biomedical applications due to the low yielding strength and poor ductility. However, the present work shows a promising method on the design of β-type Ti alloys with modulus equivalent to that of human bones. It is believed that the ultralow Young's modulus together with better combined mechanical properties can be realized by optimizing the composition and the thermomechanical processing parameters, and further research is underway.

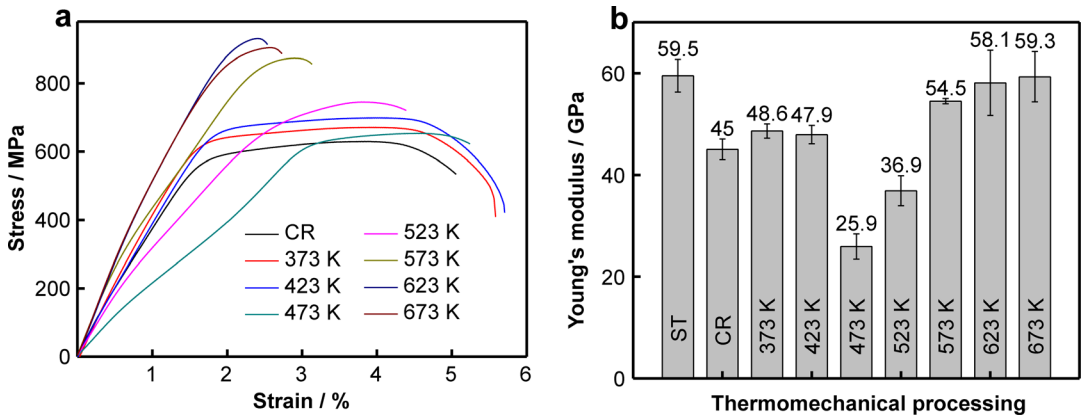

Fig. 5 **a** Tensile stress–strain curves and **b** corresponding Young's modulus of specimens subjected to different thermomechanical processing

4 Conclusion

The phase transformations of a cold-rolled Ti38Nb alloy during annealing were investigated by SXRD, and their influence on the Young's modulus was revealed. The Ti38Nb alloy with β stabilizer concentration below β_c consisted of dual β + α″ phases in ST and CR states. After annealing at 373 and 423 K for 30 min, the phase constituent remained similar to that in CR state. As a result, the Young's modulus kept almost unchanged after annealing. After annealing at 473 K for 30 min, the specimen was composed of dominate β phase together with a trace of α″ and ω phases. An ultralow Young's modulus of 25.9 GPa was realized due to the stabilization of the β phase to room temperature by high-density dislocations. After annealing at 523 and 573 K for 30 min, the specimens consisted of β + ω_{iso} and β + ω_{iso} + α phases, respectively. The precipitation of high modulus ω_{iso} and/or α phases leads to a significant increase in Young's modulus to 36.9 and 54.5 GPa, respectively. After annealing at 623 and 673 K for 30 min, the amount of α precipitates increased clearly, while the Young's modulus remained steadily. The increase in Young's modulus by the precipitation of the α phase was compensated by the dissolution of the ω_{iso} phase.

Acknowledgements This work was financially supported by the Fundamental Research Funds for the Central Universities (No. 2017QNA04). Qing-Kun Meng thanks Prof. Yu-chen Karen Chen-Wiegart at Stony Brook University and Dr. Jianming Bai, Dr. Hui Zhong and Dr. Sanjit Ghose at National Synchrotron Light Source II for their assistance in the synchrotron experiments. This research used 28-ID-2 (XPD) beamline of the National Synchrotron Light Source II, a U.S. Department of Energy (DOE) Office of Science User Facility operated for the DOE Office of Science by Brookhaven National Laboratory under Contract No. DE-SC0012704.

References

[1] Niinomi M, Nakai M, Hieda J. Development of new metallic alloys for biomedical applications. Acta Biomater. 2012;8(11):3888.
[2] Geetha M, Singh AK, Asokamani R, Gogia AK. Ti based biomaterials, the ultimate choice for orthopaedic implants—a review. Prog Mater Sci. 2009;54(3):397.
[3] Chen LY, Cui YW, Zhang LC. Recent development in beta titanium alloys for biomedical applications. Metals. 2020;10(9):1139.
[4] Niinomi M. Mechanical biocompatibilities of titanium alloys for biomedical applications. J Mech Behav Biomed Mater. 2008;1(1):30.
[5] Pellizzari M, Jam A, Tschon M, Fini M, Lora C, Benedetti M. A 3D-printed ultra-low Young's modulus β-Ti alloy for biomedical applications. Materials. 2020;13(12):2792.
[6] Sumner DR, Turner TM, Igloria R, Urban RM, Galante JO. Functional adaptation and ingrowth of bone vary as a function of hip implant stiffness. J Biomech. 1998;31(10):909.
[7] Nagoshi T, Yasuda T, Otaki N, Tahara M, Hosoda H, Sone M. Evaluation of the shape memory effect by micro-compression testing of single crystalline Ti-27Nb Ni-free alloy. Materials. 2020;13(1):110.
[8] Zhao X, Niinomi M, Nakai M, Hieda J. Beta type Ti–Mo alloys with changeable Young's modulus for spinal fixation applications. Acta Biomater. 2012;8(5):1990.
[9] Zhou YL, Niinomi M. Microstructures and mechanical properties of Ti–50mass% Ta alloy for biomedical applications. J Alloys Compd. 2008;466(1):535.
[10] Hanada S, Masahashi N, Jung TK, Miyake M, Sato YS, Kokawa H. Effect of swaging on Young's modulus of β Ti–33.6Nb–4Sn alloy. J Mech Behav Biomed Mater. 2014;32:310.
[11] Meng Q, Wang K, Li H, Guo S, Wei F, Qi J, Sui Y, Zhao X. Single crystal shear moduli of β-phase stabilized by thermo-mechanical treatment in TiNbSn alloys with ultralow elastic modulus. Mater Lett. 2021;285:129103.
[12] Meng Q, Guo S, Liu Q, Hu L, Zhao X. A β-type TiNbZr alloy with low modulus and high strength for biomedical applications. Prog Nat Sci. 2014;24(2):157.
[13] Marczewski M, Miklaszewski A, Maeder X, Jurczyk M. Crystal structure evolution, microstructure formation, and properties of mechanically alloyed ultrafine-grained Ti-Zr-Nb alloys at 36≤Ti≤70 (at%). Materials. 2020;13(3):587.
[14] Niinomi M. Fatigue performance and cyto-toxicity of low rigidity titanium alloy, Ti–29Nb–13Ta–4.6Zr. Biomaterials. 2003;24(16):2673.
[15] Li BQ, Li CL, Wang ZX, Lu X. Preparation of Ti–Nb–Ta–Zr alloys for load-bearing biomedical applications. Rare Met. 2019;38(6):571.
[16] Hao YL, Li SJ, Sun SY, Zheng CY, Yang R. Elastic deformation behaviour of Ti–24Nb–4Zr–79Sn for biomedical applications. Acta Biomater. 2007;3(2):277.
[17] Li X, Ye S, Yuan X, Yu P. Fabrication of biomedical Ti-24Nb-4Zr-8Sn alloy with high strength and low elastic modulus by powder metallurgy. J Alloys Compd. 2019;772:968.
[18] Banerjee D, Williams JC. Perspectives on titanium science and technology. Acta Mater. 2013;61(3):844.
[19] Moffat DL, Larbalestier DC. The compctition between martensite and omega in quenched Ti-Nb alloys. Metall Trans A. 1988;19(7):1677.
[20] Kim HY, Ikehara Y, Kim JI, Hosoda H, Miyazaki S. Martensitic transformation, shape memory effect and superelasticity of Ti–Nb binary alloys. Acta Mater. 2006;54(9):2419.
[21] Qu WT, Gong H, Wang J, Nie YS, Li Y. Martensitic transformation, shape memory effect and superelasticity of Ti–*x*Zr–(30–*x*)Nb–4Ta alloys. Rare Met. 2019;38(10):965.
[22] Nejezchlebová J, Janovská M, Sedlák P, Šmilauerová J, Stráský J, Janeček M, Seiner H. Elastic constants of β-Ti15Mo. J Alloys Compd. 2019;792:960.
[23] Devaraj A, Nag S, Srinivasan R, Williams REA, Banerjee S, Banerjee R, Fraser HL. Experimental evidence of concurrent compositional and structural instabilities leading to ω precipitation in titanium–molybdenum alloys. Acta Mater. 2012;60(2):596.
[24] Ng HP, Devaraj A, Nag S, Bettles CJ, Gibson M, Fraser HL, Muddle BC, Banerjee R. Phase separation and formation of omega phase in the beta matrix of a Ti–V–Cu alloy. Acta Mater. 2011;59(8):2981.
[25] Hao YL, Yang R, Niinomi M, Kuroda D, Zhou YL, Fukunaga K, Suzuki A. Young's modulus and mechanical properties of Ti-29Nb-13Ta-4.6Zr in relation to α″ martensite. Metall Mater Trans A. 2002;33(10):3137.
[26] Ho WF, Ju CP, Lin JH. Structure and properties of cast binary Ti-Mo alloys. Biomaterials. 1999;20(22):2115.

[27] Tane M, Akita S, Nakano T, Hagihara K, Umakoshi Y, Niinomi M, Mori H, Nakajima H. Low Young's modulus of Ti–Nb–-Ta–Zr alloys caused by softening in shear moduli c′ and c44 near lower limit of body-centered cubic phase stability. Acta Mater. 2010;58(20):6790.
[28] Abdel-Hady M, Hinoshita K, Morinaga M. General approach to phase stability and elastic properties of β-type Ti-alloys using electronic parameters. Scr Mater. 2006;55(5):477.
[29] Zhang K, Dong HB, Jiang ZY, Shi S, Liu HX. Effects of cold-deformation and aging process on microstructure and properties of TB8 titanium alloy. Chin J Rare Met. 2019;43(9):904.
[30] Sun F, Hao YL, Nowak S, Gloriant T, Laheurte P, Prima F. A thermo-mechanical treatment to improve the superelastic performances of biomedical Ti–26Nb and Ti–20Nb–6Zr (at%) alloys. J Mech Behav Biomed Mater. 2011;4(8):1864.
[31] Kuroda PAB, Lourenço ML, Correa DRN, Grandini CR. Thermomechanical treatments influence on the phase composition, microstructure, and selected mechanical properties of Ti–20Zr–Mo alloys system for biomedical applications. J Alloys Compd. 2020;812:152108.
[32] Li HJ, Yu Y, Song XY, Ye WJ, Hui SX. Thermal deformation behavior and processing map of a new type of Ti-6554 alloy. Chin J Rare Met. 2020;44(5):462.
[33] Sheremetyev V, Kudryashova A, Dubinskiy S, Galkin S, Prokoshkin S, Brailovski V. Structure and functional properties of metastable beta Ti-18Zr-14Nb (at.%) alloy for biomedical applications subjected to radial shear rolling and thermomechanical treatment. J Alloys Compd. 2018;737:678.
[34] Mantani Y, Tajima M. Phase transformation of quenched α″ martensite by aging in Ti–Nb alloys. Mater Sci Eng A. 2006;438–440:315.
[35] Lopes ESN, Cremasco A, Afonso CRM, Caram R. Effects of double aging heat treatment on the microstructure, Vickers hardness and elastic modulus of Ti–Nb alloys. Mater Charact. 2011;62(7):673.
[36] Ping DH, Cui CY, Yin FX, Yamabe-Mitarai Y. TEM investigations on martensite in a Ti–Nb-based shape memory alloy. Scr Mater. 2006;54(7):1305.
[37] Zhu Y, Meng Q, Guo S, Qi L, Xiao W, Ping D, Zhao X. Anomalous phase stability of surface and interior in a metastable Ti-Nb-Zr alloy. Mater Lett. 2016;169:210.
[38] Zhao CH, Kisslinger K, Huang XJ, Lu M, Camino F, Lin CH, Yan HF, Nazaretski E, Chu Y, Ravel B, Liu MZ, Chen-Wiegart YCK. Bi-continuous pattern formation in thin films via solid--state interfacial dealloying studied by multimodal characterization. Mater Horizons. 2019;6(10):1991.
[39] Zhu ZW, Xiong CY, Wang J, Li RG, Ren Y, Wang YD, Li Y. In situ synchrotron X-ray diffraction investigations of the physical mechanism of ultra-low strain hardening in Ti-30Zr-10Nb alloy. Acta Mater. 2018;154:45.
[40] Zhao C, Wada T, De Andrade V, Gürsoy D, Kato H, Chen-Wiegart YCK. Imaging of 3D morphological evolution of nanoporous silicon anode in lithium ion battery by X-ray nano-tomography. Nano Energy. 2018;52:381.
[41] Lin CH, Topsakal M, Sun K, Bai J, Zhao C, Dooryhee E, Northrup P, Gan H, Lu D, Stavitski E, Chen-Wiegart YCK. Operando structural and chemical evolutions of TiS_2 in Na-ion batteries. J Mater Chem A. 2020;8(25):12339.
[42] Prescher C, Prakapenka VB. DIOPTAS: a program for reduction of two-dimensional X-ray diffraction data and data exploration. High Press Res. 2015;35(3):223.
[43] Chen W, Sun Q, Xiao L, Sun J. Deformation-induced grain refinement and amorphization in Ti-10V-2Fe-3Al alloy. Metall Mater Trans A. 2012;43(1):316.
[44] Yang Y, Li GP, Cheng GM, Li YL, Yang K. Multiple deformation mechanisms of Ti–22.4Nb–0.73Ta–2.0Zr–1.34O alloy. Appl Phys Lett. 2009;94(6):061901.
[45] Meng Q, Guo S, Ren X, Xu H, Zhao X. Possible contribution of low shear modulus C44 to the low Young's modulus of Ti-36Nb-5Zr alloy. Appl Phys Lett. 2014;105(13):131907.
[46] Guo S, Meng Q, Zhao X, Wei Q, Xu H. Design and fabrication of a metastable β-type titanium alloy with ultralow elastic modulus and high strength. Sci Rep. 2015;5:14688.
[47] Meng Q, Li H, Wang K, Guo S, Wei F, Qi J, Sui Y, Shen B, Zhao X. In situ synchrotron X-ray diffraction investigations of the nonlinear deformation behavior of a low modulus β-Type Ti36Nb5Zr alloy. Metals. 2020;10(12):1619.
[48] Matsumoto H, Watanabe S, Hanada S. Beta TiNbSn alloys with low Young's modulus and high strength. Mater Trans. 2005;46(5):1070.
[49] Tane M, Akita S, Nakano T, Hagihara K, Umakoshi Y, Niinomi M, Nakajima H. Peculiar elastic behavior of Ti–Nb–Ta–Zr single crystals. Acta Mater. 2008;56(12):2856.
[50] Al-Zain Y, Kim HY, Hosoda H, Nam TH, Miyazaki S. Shape memory properties of Ti–Nb–Mo biomedical alloys. Acta Mater. 2010;58(12):4212.
[51] Otsuka K, Ren X. Physical metallurgy of Ti–Ni-based shape memory alloys. Prog Mater Sci. 2005;50(5):511.
[52] Meng Q, Zhang J, Huo Y, Sui Y, Zhang J, Guo S, Zhao X. Design of low modulus β-type titanium alloys by tuning shear modulus C44. J Alloys Compd. 2018;745:579.
[53] Zheng Y, Alam T, Banerjee R, Banerjee D, Fraser HL. The influence of aluminum and oxygen additions on intrinsic structural instabilities in titanium-molybdenum alloys. Scr Mater. 2018;152:150.
[54] Choudhuri D, Zheng Y, Alam T, Shi R, Hendrickson M, Banerjee S, Wang Y, Srinivasan SG, Fraser H, Banerjee R. Coupled experimental and computational investigation of omega phase evolution in a high misfit titanium-vanadium alloy. Acta Mater. 2017;130:215.
[55] Bönisch M, Calin M, Waitz T, Panigrahi A, Zehetbauer M, Gebert A, Skrotzki W, Eckert J. Thermal stability and phase transformations of martensitic Ti-Nb alloys. Sci Technol Adv Mater. 2013;14(5):055004.
[56] Nag S, Banerjee R, Srinivasan R, Hwang JY, Harper M, Fraser HL. ω-Assisted nucleation and growth of α precipitates in the Ti–5Al–5Mo–5V–3Cr–0.5Fe β titanium alloy. Acta Mater. 2009;57(7):2136.
[57] Guo S, Zhang J, Cheng X, Zhao X. A metastable β-type Ti–Nb binary alloy with low modulus and high strength. J Alloys Compd. 2015;644:411.
[58] Guo S, Shi Y, Liu G, Wu R, Luo R, Peng CT, Meng Q, Cheng X, Zhao X. Design and fabrication of a (β+α″) dual-phase Ti-Nb-Sn alloy with linear deformation behavior for biomedical applications. J Alloys Compd. 2019;805:517.
[59] Guo S, Meng Q, Liao G, Hu L, Zhao X. Microstructural evolution and mechanical behavior of metastable β-type Ti–25Nb–2Mo–4Sn alloy with high strength and low modulusMicrostructural evolution and mechanical behavior of metastable β-type Ti–25Nb–2Mo–4Sn alloy with high strength and low modulus. Prog Nat Sci. 2013;23(2):174.
[60] Meng Q, Liu Q, Guo S, Zhu Y, Zhao X. Effect of thermo-mechanical treatment on mechanical and elastic properties of Ti–36Nb–5Zr alloy. Prog Nat Sci. 2015;25(3):229.
[61] Bönisch M, Panigrahi A, Calin M, Waitz T, Zehetbauer M, Skrotzki W, Eckert J. Thermal stability and latent heat of Nb–rich martensitic Ti-Nb alloys. J Alloys Compd. 2017;697:300.